Heat losses in a trapezoidal cavity receiver of a linear Fresnel collector: A CFD approach

Sergio Alcalde-Morales [a,b], Loreto Valenzuela [a,*], J.J. Serrano-Aguilera [b]

[a] CIEMAT – Plataforma Solar de Almería, Crta. Senes, km. 4.5, 04200, Tabernas (Almería), Spain
[b] Universidad de Málaga, Escuela de Ingenierías Industriales, Campus de Teatinos, s/n, 29071, Málaga, Spain

A R T I C L E I N F O

A B S T R A C T

This paper presents a thermal study of a cavity receiver designed for a Fresnel-type linear solar collector (LFC). The study utilizes a two-dimensional computational fluid dynamics (CFD) model implemented in ANSYS Fluent. The thermal behavior of air inside the cavity for a Fresnel collector is extensively examined. The receiver consists of a trapezoidal cavity with a set of six parallel absorber tubes, through which a thermal fluid circulates. The cavity has aluminum reflectors on the inner walls and glass window closing the aperture facing the primary reflectors of the solar collector. The two-dimensional numerical model represents a cross-section of the receiver, and aims to provide numerical results that allow to provide algebraic correlations for predicting heat losses in the receiver from the wall temperature of each of the six individual absorber tubes that compose it. The developed model is transient, utilizing the k-ε turbulent model. In addition, the study is completed with an analysis of the behavior of the air surrounding and inside the cavity, to evaluate its thermal performance. For this purpose, the velocity and temperature contours obtained with the two-dimensional model are discussed. Correlations are obtained to know the heat flux between the tubes and the heat loss through the window for any combination of temperatures for each pair of tubes, which has not been yet studied in the literature. The study reveals that radiative losses contribute to 81% of the total heat losses, with the outer tubes temperature being the main responsible for these losses. Furthermore, a dimensionless analysis examines the relationship between the Nusselt and Rayleigh numbers in comparison to reference problems based on canonical geometries dominated by buoyancy-driven flows. The performance is found to be similar to that of a downward hot flat plate.

1. Introduction

Fresnel collectors, along with parabolic trough collectors, are the two most technically and commercially developed types of line-focusing concentrated solar thermal technology. A linear Fresnel solar collector (LFC) consists of an optical concentrator made up of rows of flat or slightly curved reflectors called primary reflector, which are located at the ground level. These reflectors direct sunlight onto one or more receiver tubes and may optionally include a secondary reflector at the height of the receiver. The primary reflector follows the sun during the day, while the receiver remains fixed at a height above the plane formed by the primary reflectors [1].

In the last decade, several innovative Fresnel collectors have been proposed, especially in compact sizes, to be integrated into solar

---

systems to supply heat to industrial processes [2].

The main objective of these developments has been to enhance the technology's competitiveness compared to the other concentrating solar thermal system, such as parabolic troughs. New developments in Fresnel reflector systems, that aim to improve optical and thermal performance can be classified into two groups. One group focuses on developing designs that involve innovations in the optical concentrator and designs with new receiver configurations. The second group, which is the focus of this work, presents designs and previous studies conducted by other authors.

The thermal performance of receiver designs for LFC has been studied by several authors, considering different modeling approaches and complexity. In the case of cavity receivers, one common approach followed in some studies is the simplification of the geometry to a hot plate, or similar, to study the heat losses from the receiver to the ambient. This is the case of Reynolds et al. [3], where the thermal behavior of a trapezoidal cavity is simulated assuming a constant temperature of the top cover (isothermal condition), following an approach of the original problem: a bundle of tubes placed on the top side of the cavity, inside the insulation. The side walls of the cavity are modeled as convection boundaries (convection coefficients are imposed), inside and outside the cavity. The bottom surface is modeled as a combined convection/radiation boundary, using heat transfer coefficients obtained experimentally. This study was conducted using ANSYS Fluent, considering laminar flow within the cavity. In Singh et al. [4], a trapezoidal cavity receiver is also modeled, where the absorber tubes are placed beneath the cavity top wall. The work focuses on one hand, on the impact that the paint applied on the absorber tubes surface has on heat losses. On the other hand, on the value of heat losses depending on whether a single or double glass cover is used in the lower part of the cavity. To model heat transfer between the absorber tubes and the inner glass surface, the tubes bundle is simplified as a flat plate. The flat plate representing the absorber pipes is at a constant temperature in this study. Saxena et al. [5] studied a similar case, but carrying out several simulations with different temperatures for the isothermal top cover and different aspect ratios of the cavity. The aim is to obtain non-dimensional correlations as a function of non-dimensional parameters and geometrical characteristics.

Façao et al. [6] proposes an ANSYS Fluent CFD model, where absorber tubes are included, by means of a steady-state solver with laminar flow. A heat transfer coefficient related to heat losses is obtained. The tubes are supposed to be at the same temperature. All the aforementioned works are based on the Boussinesq model, that is, variation of density is only taken into account in the momentum equation, being considered constant in the others. Manikumar et al. [7] studied the overall heat loss coefficient of a trapezoidal cavity with and without a plate under the absorber tubes and analyzed the effect of black chrome coating on the absorber surface. A numerical model is developed by using ANSYS Workbench and considering a steady-state two-dimensional non-Boussinesq model. A similar model for a trapezoidal cavity is developed in the work of Natarajan et al. [8], where a two-dimensional non-Boussinesq steady-state model is considered, imposing heat losses coefficients in the outer surfaces assuming a laminar airflow. They studied the thermal performance of the air inside the cavity, obtaining contours of temperature and heat losses as a function of the aspect ratio of the trapezoidal cavity. In the study by Reddy et al. [9] there are changes in the modeling approach to regarding the previously mentioned. A steady state is assumed too, but air turbulent flow is imposed and solved by the standard renormalization-group (RNG) $k - \varepsilon$. Besides, external air is solved too, so external heat losses coefficients are not needed.

Unlike the previous works, single-tube absorbers have also been under study. In the work of Lopez Nuñez [10], a compound parabolic concentrator along with a single-tube receiver is analyzed. The numerical model is solved considering steady-state conditions, laminar flow and variable air properties (in terms of entropy) inside the optical concentrator. Boussinesq simplification is considered, the fluid domain includes the mirrors, and the generation of entropy is studied around the surfaces. In the work of
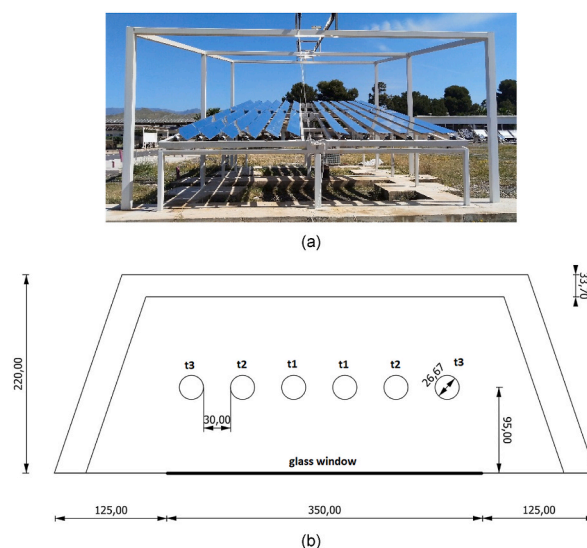
Fig. 1. LFC prototype developed at PSA: (a) general view during flux measurement tests [14] and (b) schematic cross-sectional view of the cavity receiver. Dimensions are in mm.

Velazquez et al. [11] meanwhile, a numerical investigation over a LFC with a monotube receiver (without a secondary concentrator or trapezoidal cavity) is carried out. A finite differences scheme is developed in order to solve the equations, including a numerical integration over the transversal axis.

A numerical thermal analysis of a cavity receiver for a LFC prototype is presented in this article (see Fig. 1). The solar collector system has been developed at Plataforma Solar de Almería (PSA) [12,13]. The receiver is composed of a bundle of parallel absorber tubes installed inside a trapezoidal cavity with an aperture facing downwards to the primary reflectors, where there is a glass window enclosing the cavity. The aim of the presented study is to obtain algebraic correlations by means of a two-dimensional CFD numerical model for predicting heat losses as a function of absorber tubes temperature. These numerical correlations will be of interest to be applied in future works for one-dimensional numerical models. They will make it possible to study the thermo-hydraulic behavior of solar fields using LFCs as the one designed. With the correlations obtained, it will be possible to predict heat losses in this cavity receiver whatever the tube's temperature is. It is convenient to note that these type of correlations have not been reported in the literature yet.

Section 2 of this manuscript presents the main physical characteristics of the receiver and the numerical methodology applied to perform the study, whereas section 3 summarizes the numerical results obtained. The article ends with conclusions and some remarks related to future work.

2. Materials and methods

2.1. Lineal-Fresnel collector's receiver geometry

The solar receiver analyzed is composed of a double loop with 3 tubes each, so that, in the cross-section of the receiver there are 6 parallel $1''$ of outer diameter (OD) stainless steel pipe tubes (see Fig. 1(b)). The tube bundle is installed inside a trapezoidal cavity formed by a sandwich panel consisting of an outer aluminum panel, a layer of insulating material and aluminum mirrors on the inner walls of the cavity (sides and top), as well as a glass window to protect the cavity aperture in which the tube bundle is enclosed.

As previously mentioned, the goal of the numerical study is to obtain correlations to calculate heat fluxes (in W/m) in each of the absorber tubes and through the glass to the ambient. Heat fluxes are modeled as a function of the temperature of the absorber tubes and the ambient temperature, as follows:

$$q_i = f_i(T_1, T_2, T_3, T_{amb}) \tag{1}$$

where i is an index corresponding to each pair of tubes (there are three pair of tubes), i.e. t_1, t_2 or t_3, (tubes number) and T_1, T_2 and T_3 (temperature of the tubes) stand for the temperature of the wall of each pair of tubes which are numbered from 1 to 3 starting from the center of the receiver to the left or right of the bundle. It is convenient to note that T_{amb} represents the ambient temperature.

2.2. Methodology

The ANSYS Fluent software [15] is used to carry out a set of simulations characterized by a combination of temperatures for T_1, T_2 and T_3 within the operating temperature range of the system, so that heat losses can be evaluated. The absorber tubes temperature considered ranges from 300 K to 600 K, with 50 K increments, while the ambient temperature is maintained constant at 300 K. This leads to 343 cases, where heat fluxes through the absorber tubes and glass window are evaluated. The working temperature range considered covers the current design conditions of the receiver manufactured for the LFC prototype built at PSA.

2.3. Governing equations

The problem is governed by transient Navier-Stokes equations. The equation for the conservation of mass is written as shown in Eq. (2), which represents the differential form of the mass conservation equation.

$$\frac{\partial \rho}{\partial t} + \nabla \cdot \rho \, \vec{v} = 0 \tag{2}$$

Conservation of momentum is described by Eq. (3) where p is the static pressure, τ is the stress tensor given by Eq. (5) and $\rho \, \vec{g}$ is the gravitational body force, with no extra external body forces taken into account.

$$\frac{\partial \rho \, \vec{v}}{\partial t} + \nabla \cdot (\rho \, \vec{v} \, \vec{v}) = -\nabla p + \nabla \cdot (\tau) + \rho \, \vec{g} \tag{3}$$

The energy equation is solved as given in Eq. (4), where no sources of energy are considered. The effective conductivity is given by $k_{eff} = k + k_t$, with k_t as the turbulent thermal conductivity, defined according to the turbulence model being used (see section 2.3.2).

Since temperature differences are higher than 100 K, non-Boussinesq model are recommended. So, variation of air density has been taken into account in the equations, following the ideal-gas equation given by Eq. (6). Besides, variation of viscosity and conductivity of the air, as a function of temperature, has been also taken into account.

$$\frac{\partial}{\partial t}\rho\left(e+\frac{1}{2}v^2\right)+\nabla\cdot\left(\rho\left(h+\frac{v^2}{2}\right)\vec{v}\right)=\nabla\cdot\left(k_{eff}\nabla T+\tau\cdot\vec{v}\right) \tag{4}$$

The stress tensor is given by Eq. (5)

$$\tau=\mu\left(\left(\Delta\vec{v}+\Delta\vec{v}^T\right)-\frac{2}{3}\tau\cdot\vec{v}I\right) \tag{5}$$

where τ is the molecular viscosity, and I is the unit tensor [15].

The ideal-gas equation is given by Eq. (6),

$$\rho=\frac{pM}{RT} \tag{6}$$

where $R = 8.314$ J/(K·mol) is the universal gas constant and $M = 0.02897$ kg/mol is the molar mass of air.

The variation of the viscosity concerning the temperature is modeled according to Sutherland's theory for viscosity, applying the three-coefficient method [16], whose expression is given by Eq. (7),

$$\frac{\mu}{\mu_0}=\left(\frac{T}{T_0}\right)^{3/2}\cdot\left(\frac{T_0+S}{T+S}\right) \tag{7}$$

where T_0 is a reference air temperature ($T_0 = 273.15$ K), μ_0 is the viscosity of the air at reference temperature ($\mu_0 = 1.72\cdot10^{-5}$ kg/(m·s)). S is the Sutherland temperature, which takes a value of 110 K.

2.3.1. Radiative model

The surface-to-surface radiation model has been used to obtain radiation exchange inside and outside the cavity. ANSYS Fluent's S2S radiation model assumes the surfaces to be gray and diffuse. Emissivity and absorptivity are independent of wavelength. Also, by Kirchoff's law, emissivity equals absorptivity. The energy flux leaving each surface is composed of directly emitted and reflected energy. The reflected energy is expressed in terms of the energy flux leaving all other surfaces.

$$q_{out,k}=\varepsilon_k\sigma T_k^4+\rho_k q_{in,k} \tag{8}$$

where $q_{out,k}$ is the energy flux leaving the surface and $q_{in,k}$ is the energy flux incident on the surface from the surroundings. This energy is a direct function of view factor F_{jk}, the fraction of energy leaving surface k that is incident on surface j. Equation (8) can be written in terms of the view factors as follow:

$$q_{out,k}=\varepsilon_k\sigma T_k^4+\rho_k\sum_{j=1}^{N}q_{out,j}F_{kj} \tag{9}$$

where N is the total number of surfaces.

2.3.2. Turbulence model

Rayleigh number (see Eq. (10)) governs the regime of fluid flow, it describes the behavior when the mass density of the fluid is non-uniform. By definition, it is the ratio of the time scale for diffusive thermal transport to the time scale for convective thermal transport at the characteristic velocity [17].

$$Ra=\frac{g\beta\Delta TL_c^3}{v\alpha} \tag{10}$$

In the case study presented, natural convection occurs above the absorber tubes inside the cavity, being not favored under the tubes where viscous forces stabilize the fluid (air). To characterize the flow regime condition inside the cavity for the working temperature range defined for the receiver, $300 < T < 600$ K, the Rayleigh number is calculated at a mid-temperature within this range, i.e. at 450 K. In Eq. (10), L_c is the characteristic length, corresponding to the diameter of each tube (26.67 mm), ΔT is the difference between the absorber tube temperature and the ambient temperature. Considering these values, the Rayleigh number obtained is $Ra = 2.75\cdot10^6$, higher than 10^5, so the problem is dominated by the turbulence.

The adopted turbulence model is the $k-\varepsilon$, which uses two equations to determine the turbulence scale and the time scale, using the RNG modification. The value of k refers to the kinetic energy associated with turbulence and ε refers to the dissipation ratio. It has been found a better performance of the fluid inside the cavity by using $k-\varepsilon$ instead of using $k-\omega$ SST model in terms of stability of the oscillatory stationary solution. In the context of natural convection, where the flow is primarily driven by buoyancy forces, the RNG-based k-epsilon model can better capture the turbulence characteristics and heat transfer phenomena [18,19]. The RNG modification helps to enhance the model's performance by introducing additional physics and improving the prediction of turbulent quantities in low-Reynolds number flows. The scale elimination procedure in RNG theory results in a differential equation for turbulent viscosity, that can be imposed on ANSYS Fluent to be used in order to include low-Reynolds number effects [15]. For an appropriate treatment of the near-wall region, enhanced wall treatment, taking into account thermal effects are chosen (see section 2.7.1).

2.4. Solution method

The equations are solved by applying the SIMPLEC scheme [20], a modification of the SIMPLE scheme, which follows the same iterative steps to solve the discretized momentum equations. Both algorithms allow obtaining the velocity and pressure fields for an incompressible flow, but in the SIMPLEC the velocity correction formulas omit terms less significant than those omitted in the SIMPLE algorithm, being more efficient. The SIMPLEC scheme is chosen, due to it allows a correction in the calculations to take into account the curved zones of the domain (tubes), which is necessary to obtain greater efficiency in the whole resolution of the problem.

(a)

(c)

(b)

(d)
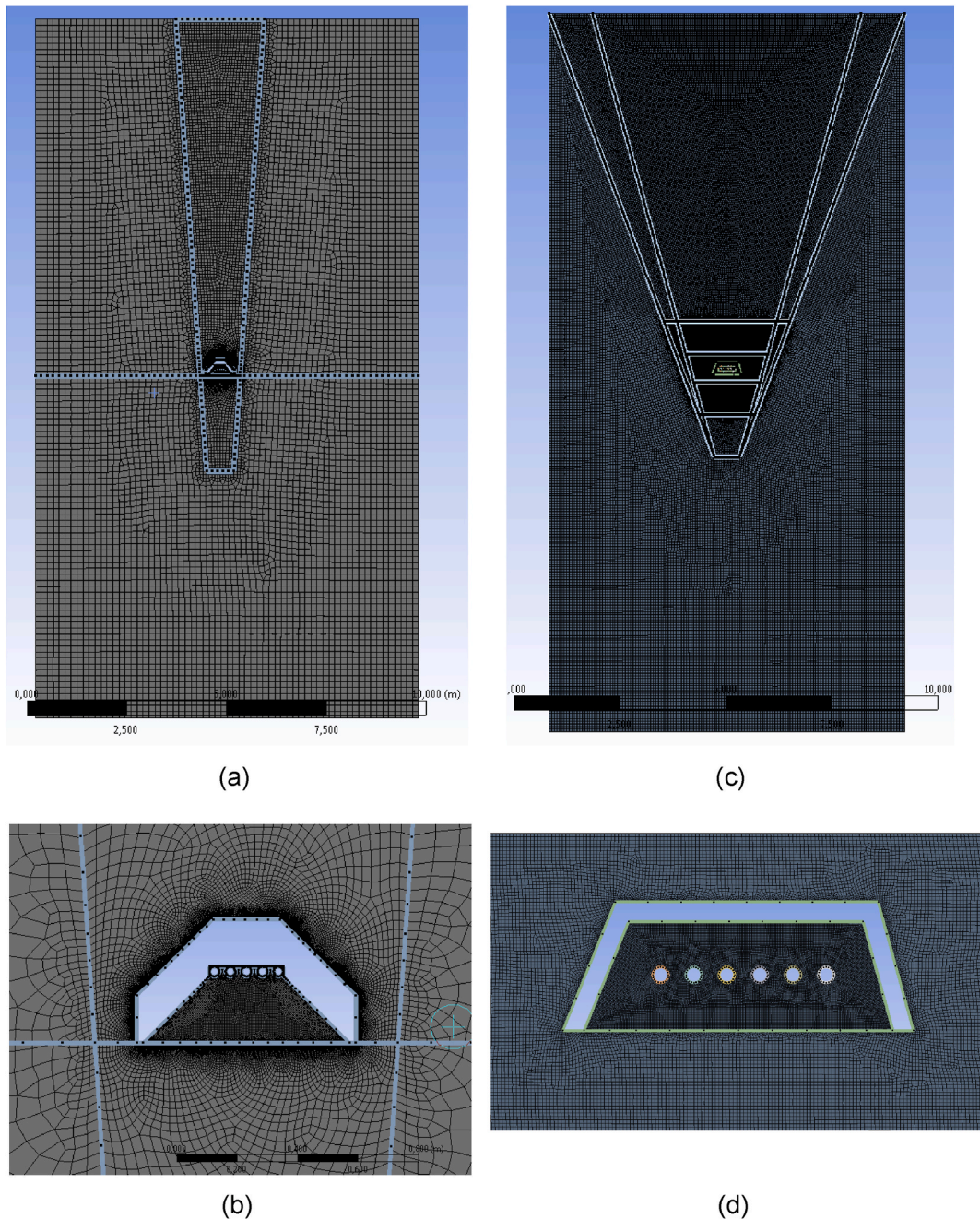
Fig. 2. Mesh of the fluid domain in the ANSYS Fluent 2D model of LFC receiver: (a) and (c) for the receiver design presented in Ref. [21], considered for validation of the modeling approach; and (b) and (d) for the cavity receiver of the LFC prototype installed at PSA.

2.5. Validation of the model

To validate the proposed model, its results have been compared to the experimental results provided by Flores et al. [21]. Fig. 2(a) and (b) show the mesh adopted to reproduce this experimental problem.

Table 1 summarizes the following results for the six cases solved, including the following: (i) the total heat loss in the cavity; (ii) the mean temperature of the air inside the cavity (T_{cavity}), and (iii) the mean temperature of the lateral surface of the cavity (T_{inner}), compared all them with the mean temperature of the tubes (T_{pipe}).

The mean errors obtained for the temperature of the air of the cavity and its lateral faces are 1.22% and 1.04% respectively. These results indicate that an appropriate approach has been followed, especially considering that a 2D model was used to model a physical 3D problem. The errors associated with heat losses are below 1% (0.98%), confirming the suitability of the modeling approach for the current application.

2.6. Initial and boundary conditions

A set of boundary conditions have been implemented in the model: absorber tubes temperature, non-slip condition on the solid surfaces, the ambient temperature set to 300 K far away from the cavity, atmospheric pressure and null-velocity in the borders of the domain. Insulation of the cavity wall is modeled as an adiabatic zone, so null heat flux is imposed. The emissivity values of the different surfaces considered in the problem are: 0.93 for the tubes surface, 0.88 for the glass cover and 1 for other surfaces.

The condition of null-velocity has been set for the outer border of the domain, so that external conditions can be reproduced. For that purpose, an extensive domain is required. On the other hand, it has been found that considering insulation as an adiabatic zone is the best choice, in order to achieve a significant reduction in computing cost, and the difference in the heat losses results is minimum, as it can be seen in Table 2. In this table, measured heat losses are highlighted as a function of selected values of T_{pipe}, which are reported in Ref. [21], and calculated for each of the approaches followed to model the cavity wall and in comparison. The results corresponding to insulation being meshed and non-meshed (contour) correspond to the ones where the cavity is an adiabatic zone. As it can be seen, if the insulation is only considered as a contour, an adequate performance at low temperatures is found. For this reason, the insulation will be considered in the modeling approach of the cavity receiver presented in this study as a contour and is not meshed (see Fig. 2(c) and (d)). Mathematically, boundary and initial condition can been expressed as follows: $P_\infty = P_{atm}$, $T_\infty = 300\,K$, $T(x_i, y_i, t) = T_i$, $u(x, y, 0) = 0$ and $u(x_j, y_j, t) = 0$, where ∞ refers to the outer borders of the domain (far field), i refers each pair of tubes and j the all the surfaces, where the non-slipt condition is imposed. Fig. 3 shows a diagram detailing the boundary conditions set inside the cavity.

2.7. Meshing

Fig. 2(c) and (d) show the fluid domain and the optimal meshing defined to model and simulate the cavity receiver of the LFC prototype installed at PSA. As it has been done for the receiver considered in the validation (see section 2.5), the mesh size is finer the closer the element is to the critical parts of the receiver (absorber tubes, cavity walls and glass cover). In addition, on the surface above the cavity, the mesh has also been refined to be able to correctly reproduce the thermal plume emanating upwards from it, which significantly influences heat losses from the cavity. Mesh size must be large enough so that the conditions imposed at the far field do not affect the solution near the cavity. To extrapolate the characteristics of the mesh to a similar problem, the aspect ratio between the size of the cavity and the size of the mesh will be obtained.

2.7.1. Near-wall treatment: y^+

To determine how the near-wall treatment is, two options are available: the use of wall functions or the utilization of a near-wall model. The first option, wall functions, allows for a lower number of nodes in the vicinity of the walls, with the requirement that y^+ value falls between 30 and 60 [15]. However, when dealing with heat transfer problems, which involve the calculation of temperature gradients and heat fluxes, the use of a near-wall model is required [15]. To solve properly the viscous sublayer, it is necessary to have a mesh with a y^+ value between 1 and 5 on the surfaces. To achieve the appropriate element size in the vicinity of the surfaces, the y^+ definition given by Eq. (11) is used:

Table 1
Validation results of the modeling approach: Comparison of CFD numerical results to experiments from Ref. [21].

T_{pipe} (K)	Heat losses (W)		T_{cavity} (K)		T_{inner} (K)	
	Experiment	Simulation	Experiment	Simulation	Experiment	Modeling
383.9	180.8	185.9	329.5	332.8	335.1	331.1
429.2	355.6	369.6	349.9	351.0	347.7	348.3
445.4	433.1	408.2	358.6	354.3	357.0	352.4
471.7	586.1	565.5	371.9	375.2	369.9	371.8
510.7	828.5	763.1	394.0	390.9	391.2	389.0
558.0	1132.5	1127.8	420.5	432.6	418.9	428.5

Table 2
Validation results of the modeling approach: Comparison of numerical results to experiments from Ref. [21].

T_{pipe} [K]	Experimental heat losses (W)	Simulated heat losses (W)		
		Insulation meshed	Insulation non-meshed	No-insulation
384.0	186.2	227.6	196.3	220.7
428.6	356.3	406.9	370.1	303.4
444.9	429.9	446.0	406.9	427.6
469.8	579.3	577.0	572.4	519.5
480.8	646.0	797.7	703.4	717.2
496.5	744.8	859.8	760.9	772.4
524.8	921.8	995.4	995.4	951.7
557.1	1128.7	1142.5	1131.5	1234.5
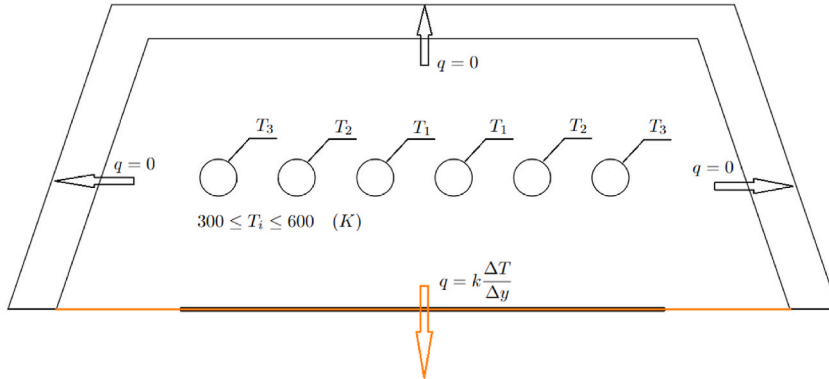
Fig. 3. Configuration of boundary conditions inside the cavity receiver.

$$y+ = \frac{yU_\tau\rho}{\mu} \tag{11}$$

where y is the length of the elements in the surface and U_τ is the characteristic transverse velocity, given by Eq. (12),

$$U_\tau = \sqrt{\frac{\tau_w}{\rho}} \tag{12}$$

being τ_w the wall shear stress, given by Eq. (13).

$$\tau_w = \frac{1}{2}C_f\rho U_\infty^2 \tag{13}$$

The friction coefficient C_f for a Reynolds number based on the diameter of a tube is given by Eq. (14), and for a flat plate is given by Eq. (15),

$$C_{f,tube} = 0.079 Re_d^{-0.25} \tag{14}$$

$$C_{f,plate} = 0.058 Re_l^{-0.2} \tag{15}$$

where Re_d is the characteristic Reynolds number for air around the tubes, while Re_l is the characteristic Reynolds number for the air close to a flat plate. Characteristic velocity is set at U_∞, being the magnitude order of the velocity obtained in preliminary works. Air

Table 3
Summary of the mesh independence test results.

Number of cells	Heat losses (W/m)	% change in heat losses
14,484	20.31	–
53,604	17.08	18.93
81,473	16.23	5.18
100,324	15.91	2.04
141,137	16.44	−3.21
202,332	16.55	0.67
211,002	16.49	0.38

properties are obtained for the maximum temperature in the cavity (600 K), which leads to the following values: $Re_d = 8.85$ and $Re_l = 2246.8$. Employing previous equations, the size of mesh elements must be such that the value of y is within the following range: 0.0020 m $< y < 0.01$ m, for absorber tubes, and 0.0029 m $< y < 0.0147$ m, for flat plate (glass cover). With these values, a mesh convergence study is carried out. A growth rate equal to 1.2 is imposed. Besides, the domain size outside the cavity must be large enough to obtain accurate results near the cavity. For this problem, it has been found that a fluid domain that is 80 times higher and 13 times wider than the cavity yields accurate results. Consequently, the dimensions of the fluid domain are 17 m × 8.4 m.

2.7.2. Mesh convergence test

With the aim of assessing the level of mesh refinement level, a convergence test has been conducted. Table 3 presents the results of this analysis, specifically displaying the convective heat losses for each case.

It can be observed that a 141,137 cells mesh, yields results that are virtually the same as those obtained with finer meshes. Furthermore, Table 3 provides the variation (%) of the results compared to the previous mesh with fewer cells.

3. Results

The main and most significant results derived from the CFD numerical simulations carried out are shown, as well as the algebraic correlations obtained through non-linear regression to calculate the heat fluxes from the absorber tubes to the glass window. The problem turns out to be transient, where a periodic behavior has been observed. Therefore, a transient solver is recommended. As a matter of example, Fig. 4 shows heat losses through the glass window of the cavity versus time for one particular case. It also shows heat fluxes through each tube. In order to have a representative value of the heat flux time series and the subsequent heat losses, the values are averaged for the last 15 s of the simulation.

Owing to the existing temperature range, radiation is the dominant heat transfer mechanism. On average, it represents 81% of the total heat losses in the cases studied. This is due to, on the one hand, by definition, radiation is proportional to the fourth power of the temperature and convection is linearly proportional to the temperature. On the other hand, the higher the temperature of the absorber tubes, the more intense the air stratification is inside the cavity (see section 3.4). In these cases, the convection is less relevant, while heat transfer by radiation increases due to the temperature rise.

3.1. Algebraic correlations for heat losses

The main interest in obtaining algebraic correlations to calculate heat losses for the LFC receiver cavity is to later consider this formulation in one-dimensional models, where the thermo-hydraulic performance of the systems will be analyzed in transient conditions. From numerical results obtained in the CFD simulations, correlations for heat fluxes in each element are obtained through non-linear regression for convection and thermal radiation separately. The correlations given by Eqs. (16)–(18), are used to model radiative heat fluxes, while the correlations given by Eqs. (19)–(21), are used to model convective heat fluxes.

The formulation considered for radiation correlations takes into account linear and fourth power terms of the temperature difference between all cavity elements. For convection, the use of cubic power term has been found to be more suitable.

In all these correlations, T_i (in K) is the temperature of each pair of tubes ($i = 1, 2, 3$) (note that both tubes of each pair are at the same temperature), and $q_{r,ti}$ and $q_{c,ti}$ represent net radiant and convective heat flux (in W/m) respectively, leaving from the pair of tubes with index i.

$$
\begin{aligned}
q_{r,t_1} = & C_{r,0} + C_{r,1} \cdot (T_1 - T_2) + C_{r,2} \cdot \left(T_1^4 - T_2^4\right) + C_{r,3} \cdot (T_1 - T_3) + \\
& C_{r,4} \cdot \left(T_1^4 - T_3^4\right) + C_{r,5} \cdot (T_1 - T_{amb}) + C_{r,6} \cdot \left(T_1^4 - T_{amb}^4\right)
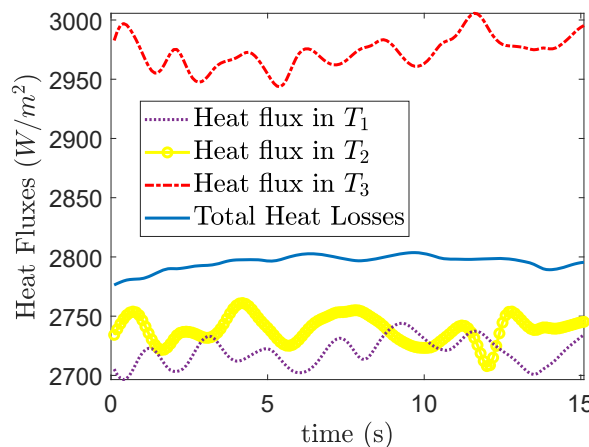\end{aligned}
\tag{16}
$$

Fig. 4. Heat fluxes inside the cavity and heat losses for $T_{tube} = 600$ K.

$$q_{r,t_2} = C_{r,0} + C_{r,1} \cdot (T_2 - T_1) + C_{r,2} \cdot \left(T_2^4 - T_1^4\right) + C_{r,3} \cdot (T_2 - T_3) +$$
$$C_{r,4} \cdot \left(T_2^4 - T_3^4\right) + C_{r,5} \cdot (T_2 - T_{amb}) + C_{r,6} \cdot \left(T_2^4 - T_{amb}^4\right) \tag{17}$$

$$q_{r,t_3} = C_{r,0} + C_{r,1} \cdot (T_3 - T_2) + C_{r,2} \cdot \left(T_3^4 - T_2^4\right) + C_{r,3} \cdot (T_3 - T_1) +$$
$$C_{r,4} \cdot \left(T_3^4 - T_1^4\right) + C_{r,5} \cdot (T_3 - T_{amb}) + C_{r,6} \cdot \left(T_3^4 - T_{amb}^4\right) \tag{18}$$

$$q_{c,t_1} = C_{c,0} + C_{c,1} \cdot (T_1 - T_2) + C_{c,2} \cdot (T_1 - T_2)^3 + C_{c,3} \cdot (T_1 - T_3) +$$
$$C_{c,4} \cdot (T_1 - T_3)^3 + C_{c,5} \cdot (T_1 - T_{amb}) + C_{c,6} \cdot (T_1 - T_{amb})^3 \tag{19}$$

$$q_{c,t_2} = C_{c,0} + C_{c,1} \cdot (T_2 - T_1) + C_{c,2} \cdot (T_2 - T_1)^3 + C_{c,3} \cdot (T_2 - T_3) +$$
$$C_{c,4} \cdot (T_2 - T_3)^3 + C_{c,5} \cdot (T_2 - T_{amb}) + C_{c,6} \cdot (T_2 - T_{amb})^3 \tag{20}$$

$$q_{c,t_3} = C_{c,0} + C_{c,1} \cdot (T_3 - T_2) + C_{c,2} \cdot (T_3 - T_2)^3 + C_{c,3} \cdot (T_3 - T_1) +$$
$$C_{c,4} \cdot (T_3 - T_1)^3 + C_{c,5} \cdot (T_3 - T_{amb}) + C_{c,6} \cdot (T_3 - T_{amb})^3 \tag{21}$$

The correlations in Eqs. (19)–(21), furthermore are useful in order to provide a better understanding of the convective transport inside the cavity. They have been formulated taking into account the temperature of all parts of the cavity that are exchanging heat (i.e. absorber tubes and glass cover). To obtain the proposed flux correlations, the CFD numerical results have been fitted using non-linear least squares. Table 4 shows the values of each fitted coefficient $C_{r,i}$ ($i = 0, 1, \ldots 6$), for modeling the radiative heat fluxes, whereas Table 5 shows the correlations coefficients $C_{c,i}$ ($i = 0, 1, \ldots 6$), for modeling the convective heat fluxes.

Given any combination of temperatures in the cavity, the total heat fluxes can be obtained by adding radiative and convective heat losses, as given by Eqs. (22) and (23) respectively. Therefore, the total heat loss in the receiver cavity is given by Eq. (24).

$$q_r = \sum_{i=1}^{3} q_{r,t_i} \tag{22}$$

$$q_c = \sum_{i=1}^{3} q_{c,t_i} \tag{23}$$

$$q = q_r + q_c \tag{24}$$

3.1.1. Influence of fluid flow direction on heat losses

Due to its practical interest, it is convenient to evaluate how each tube, its temperature and its position within the cavity contributes to heat losses. For that purpose, the evolution of heat losses has been displayed versus the combination of the temperature of the tubes. Note that in a real facility, only two scenarios can be given: $T_1 > T_2 > T_3$ (when the heat transfer fluid enters the receiver bundle through the tubes located at both sides) and $T_1 < T_2 < T_3$ (when it does it through the pair or tubes at the center, please see Fig. 1(b)). According to that, the main objective is to know what of the two cases is more convenient in terms of thermal efficiency. Figs. 5 and 6 show the evolution of the radiative and convective heat losses, q_r and q_c respectively (Eqs. (22) and (23)) as a function of some combinations of temperature in the tubes.

Blue curves (hollow circle) represent heat losses as a function of T_1 given a constant temperature for T_2 and T_3, where $T_2 < T_3$. In each case, as long as T_1 is smaller than T_2 (see vertical solid line), the second scenario (flux inlet at the center) is being represented. Alternatively, red curve (using + as symbol) represents heat losses as a function of T_3 given a constant temperature for T_1 and T_2, where $T_1 > T_2$. In each case, as long as T_3 is smaller than T_2, the first scenario (fluid flow inlet through the tubes located in both sides) is being represented. For each particular case, blue and red curves are displayed for the same combination of temperatures, so T_{pipe}, which is the average temperature of the three values of T_{tube}, is the same for both scenarios. Therefore, as long as T_1 (blue curves with hollow circles) or T_3 (red curve with "+") are smaller than T_2, both scenarios are being compared at same conditions. In other words, left part of the curves, divided by a vertical-black line, is the representative zone of the curve.

In all the cases shown in Figs. 5 and 6, the first scenario considered ($T_1 > T_2 > T_3$) leads to lower thermal energy losses, so the optimum situation is that when the heat transfer fluid enters through the pipes located at both sides of the receiver bundle.

### 3.2. Goodness of the heat losses fitting

It is of interest to describe how the provided heat losses correlations differ from the calculated numerical values by the CFD code. Table 6 shows differences between the simulation results and those obtained by evaluating the radiative and convective heat losses

Table 4
Fitted coefficients of the radiative heat fluxes algebraic correlations.

Tube	$C_{r,0}$	$C_{r,1}$	$C_{r,2} \cdot 10^{10}$	$C_{r,3}$	$C_{r,4} \cdot 10^{10}$	$C_{r,5}$	$C_{r,6} \cdot 10^9$
t_1	0.24	−0.0040	18.93	0.0194	12.21	−0.089	36.34
t_2	0.47	0.0413	19.40	0.014	19.32	−0.099	36.91
t_3	2.92	0.0725	12.34	0.066	18.98	−0.156	41.49

Table 5
Fitted coefficients of the convective heat fluxes algebraic correlations.

Tube	$C_{c,0}$	$C_{c,1}$	$C_{c,2} \cdot 10^6$	$C_{c,3}$	$C_{c,4} \cdot 10^6$	$C_{c,5}$	$C_{c,6} \cdot 10^7$
t_1	−6.27	0.52	2.10	0.52	1.88	0.12	−6.64
t_2	−4.49	0.53	1.97	0.51	1.90	0.11	−5.13
t_3	−4.17	0.52	1.88	0.52	2.00	0.11	−5.29
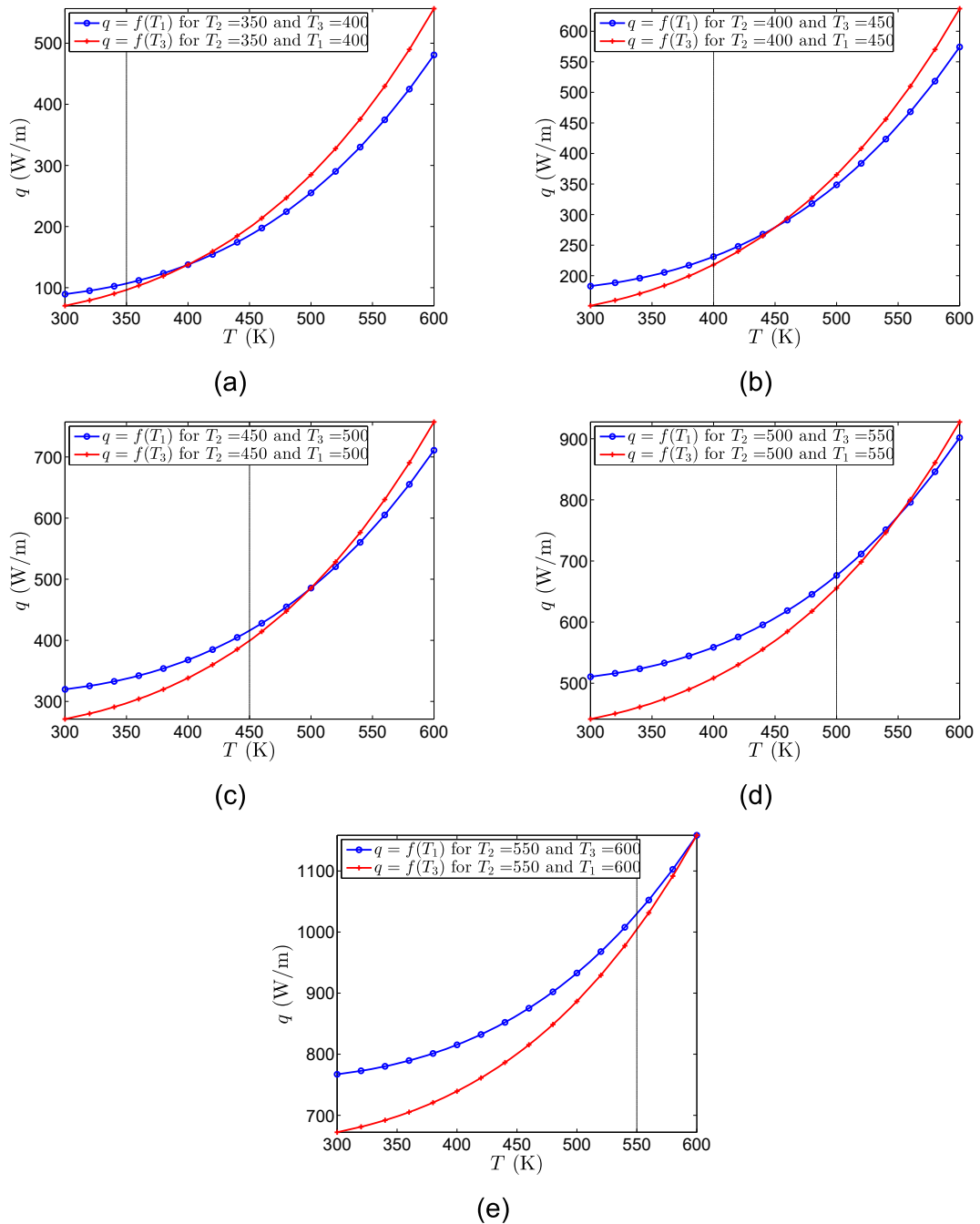
Fig. 5. Evolution of radiative heat losses as a function of the combinations of T_1, T_2 and T_3.
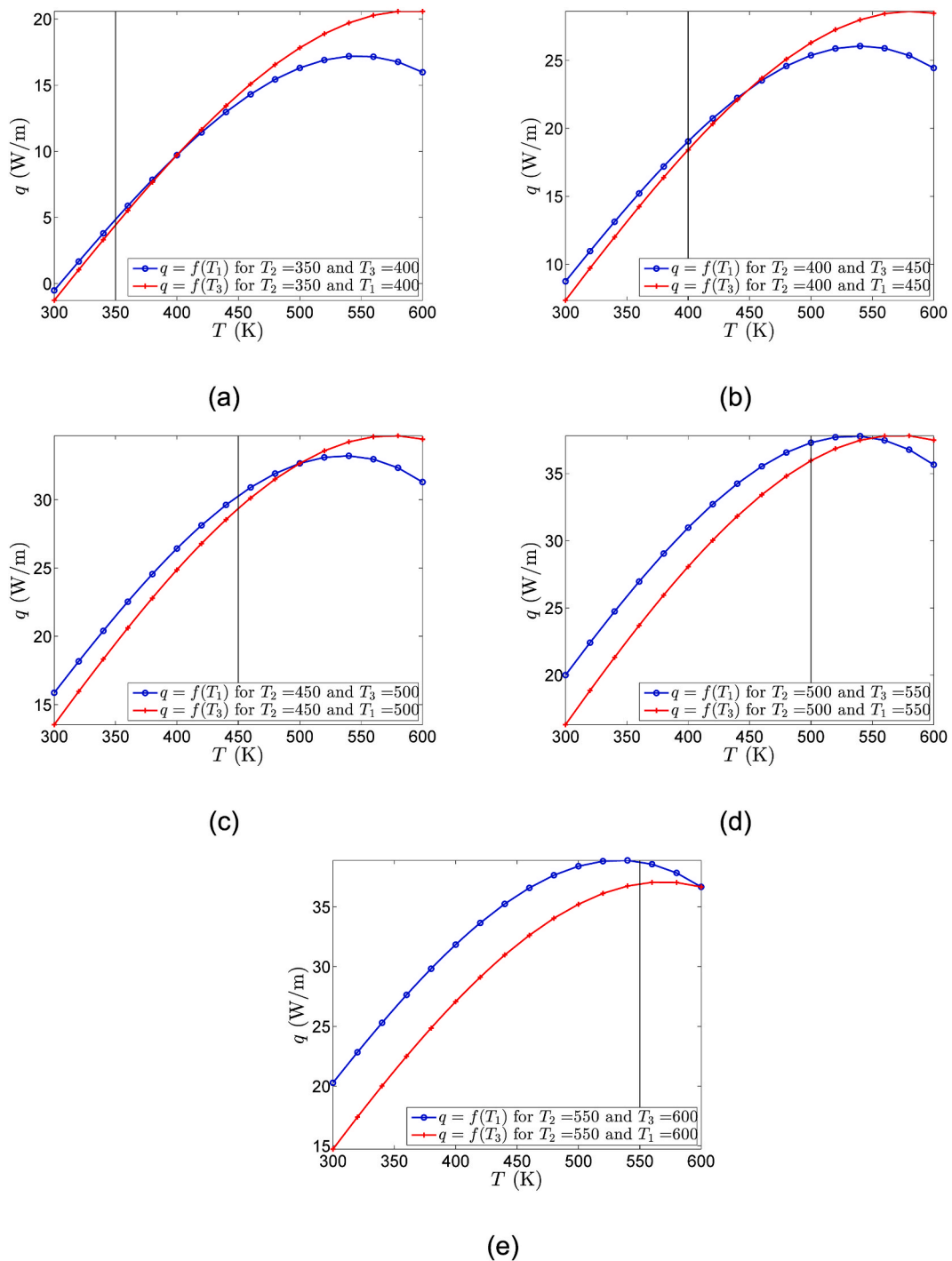
(a)

(b)

(c)

(d)

(e)

Fig. 6. Evolution of convective heat losses as a function of the combinations of T_1, T_2 and T_3.

correlations obtained by least-squares fits, using Eqs. (16)–(21) and coefficients detailed in Tables 4 and 5. To facilitate the representation and interpretation of these comparative results, the differences are displayed versus the sum of the tube temperatures T_1, T_2 and T_3. Results presented include the mean of the deviations obtained in each case (combination of temperatures that delivers the sum given) and the minimum and maximum deviations obtained from the results of 343 simulation cases analyzed.

To compare the results, the mean absolute error (MAE) is calculated for all data sets processed. That is, the mean of the errors obtained in all the cases for each tube t_i, with $i = 1, 2, 3$. Table 7 shows the mean absolute errors calculated for both radiative, MAE_r, and convective, MAE_c, heat losses. These results indicate that the correlations proposed to describe heat losses are a suitable tool to

Table 6
Representative differences of results provided by the radiative and convective heat losses correlations when compared to CFD simulations' results.

$T_1 + T_2 + T_3$ (K)	Radiative heat losses, differences (W/m)			Convective heat losses, differences (W/m)		
	Mean	Minimum	Maximum	Mean	Minimum	Maximum
900	0.5	0.2	2.9	5.0	4.7	7.0
1000	1.5	1.4	2.9	3.3	3.1	3.8
1100	1.2	1.1	1.7	3.9	3.5	4.2
1200	1.4	1.3	1.6	3.5	3.5	3.7
1300	1.9	1.7	2.2	2.9	2.7	3.2
1400	2.6	2.5	2.9	2.6	2.3	2.8
1500	2.6	2.5	2.8	3.4	3.2	3.7
1600	2.1	2.1	2.5	2.6	2.5	2.6
1700	1.6	1.5	3.4	3.7	2.9	4.1
1800	0.4	0.2	2.6	6.2	6.0	7.8

Table 7
Radiative and convective heat losses comparison in terms of mean absolute errors.

Tube	MAE_r (W/m)	MAE_r (%)	MAE_c (W/m)	MAE_c (%)
t_1	1.46	0.59	3.03	2.42
t_2	1.48	0.54	2.91	2.33
t_3	1.58	0.59	2.97	2.37

estimate them by simply using an algebraic expression in such a complex multivariate problem. The errors corresponding to the convective losses correlation are slightly higher than those for radiative losses. With regard to radiation, the MAE value is around 1.5%, whereas for convection, it goes up to 2.4%, but in any case, the correlations are acceptable for their purpose.

3.3. Comparison of heat losses in the cavity receiver

To prove the effectiveness of the thermal performance analysis of the cavity in terms of heat losses, the results are compared to findings from previous studies of similar solar collectors receivers. Specifically, the configurations proposed by Flores et al. [21] and Sahoo et al. [8] are considered under similar operation conditions. Fig. 7 depicts the heat losses calculated using the modeling approach and cavity receiver geometry presented in this study compared to the results from the two cited works [21,22] are compared, for a similar range of temperatures T_{pipe}.

In general terms, it can be reported that heat losses calculated by means of the algebraic equations proposed in this study are within the range of values reported in the works by Flores et al. [21] and Sahoo et al. [22]. However, there are some differences that can be explained as follows: Firstly, the number of tubes composing the absorber plays a significant role in heat transfer mechanisms, both to the fluid and to the surrounding environment, the latter being the case under analysis. The receiver given by Sahoo et al. [8] has the highest number of tubes, resulting in higher heat losses. This is because the surface area of the tubes in relation to the cavity size is larger, leading to more heat exchange. Conversely, the receiver proposed by Flores et al. [21], has a lower number of tubes, leading to
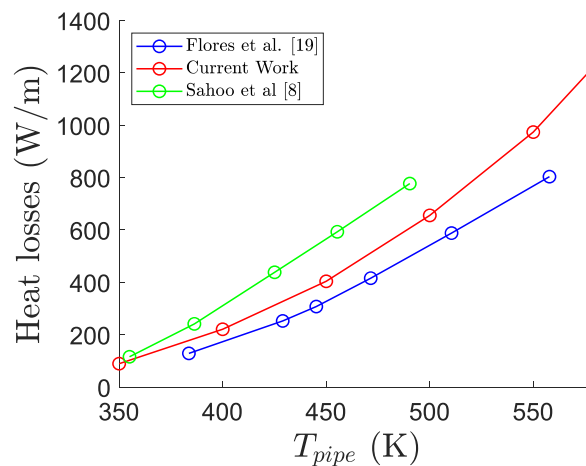
Fig. 7. Comparison of heat losses results for the cavity receiver and applying the algebraic correlations of this study and results from Flores et al. [21] and Sahoo et al. [8] with similar solar receivers.

lower heat losses.

Additionally, the positioning of the absorber tubes inside the cavity influences the air temperature distribution within the cavity environment. Placing the tube bundle higher inside the cavity reduces heat losses. When the tube bundle is located at the top of the cavity, natural convection is hindered, resulting in minimal heat losses due to convection. If the bundle of tubes is on the top of the cavity, the natural convection is impeded, so heat losses by convection are minimum. Furthermore, the radiative heat losses are affected by the form factors between the absorber tubes and the window.

3.4. Non-dimensionalisation

To provide a clearer understanding of the problem inside the cavity, a dimensionless analysis has been conducted. This analysis allows us to set a comparison with analogous problems discussed in the literature, particularly, cases where all tubes have the same temperature. Two important dimensionless numbers in buoyancy-driven flows have been considered: the Rayleigh number (Ra) defined in section 2.3.2 and the Nusselt number (Nu), which accounts for the ratio of convective to diffusive heat transfer [22] and is given in Eq. (25).

To establish a comparison between both dimensionless numbers, a canonical problem has been taken. This problem involves a flat plate with the same width as the bundle of tubes, in an environment where the infinite temperature is the temperature of the glass cover. The adopted characteristic length L_c for the Nusselt number is the width of the bundle of absorber tubes,

$$Nu = \frac{h_{conv}L_c}{k} \tag{25}$$

where h_{conv} represents the convective heat transfer coefficient, given as follows:

$$h_{conv} = \frac{q_{conv}}{\Delta T} \tag{26}$$

Note that q_{conv} (W/m^2) represents the heat fluxes from the tubes due to convection and ΔT is the difference between the tubes temperature and the glass cover temperature.

The value of the dimensionless numbers, the Nusselt number and Rayleigh number, as a function of the temperature difference between glass cover's temperature and bundle's temperature (ΔT), is presented in Fig. 8. Fig. 8(a) illustrates the relationship between the Nusselt number and ΔT, where it can be observed that the Nusselt number decreases as ΔT increases. Fig. 8(b) shows the variation of the Rayleigh number with ΔT. The Rayleigh number initially increases with ΔT until a critical value is reached, after which it starts to decrease. The drop of the Nusselt number with increasing ΔT means that higher temperature differences enhance heat transfer through conduction. The evolution of the Rayleigh number indicates that there is a critical ΔT value beyond which the time scale for diffusive thermal transport decreases due to the stratification of air inside the cavity. Additionally, considering that the conductivity of air increases with temperature, the decrease in the Rayleigh number is justified.

Fig. 9(a) shows the temperature distribution along a vertical line in the middle of the cavity for selected cases represented in Fig. 8. This plot allows for the observation of temperature gradients within the cavity. Fig. 9(b) displays the vertical component of the velocity field along a horizontal line in the middle of the cavity, between the tubes and the glass cover. This visualization enables a comparison of the intensity of convective transport for different cases. By analyzing Fig. 9(a), it can be observed that as ΔT increases, the temperature gradient becomes more pronounced, indicating enhanced diffusive transport. However, in Fig. 9(b) it can be noticed that the increase of ΔT does not lead to a significant growth of the velocity, that is related to convection. Note that all the profiles represented are virtually overlapping each other. It means that convective effects do not increase in the same manner as diffusive terms do, so there is a characteristic value of ΔT where maximum for the Rayleigh is obtained.

Since no forced convection is given inside the cavity, it is of importance to analyze the relationship between the Nusselt and Rayleigh numbers for the problem (green dots in Fig. 10). It also shows the $Nu(Ra)$ relationship for two canonical problems: (a) a hot surface facing upwards (blue dots) and (b) a hot surface facing downwards (red dots) [23]. Comparing the trend of the $Nu(Ra)$ curve for the tubes inside the cavity with the hot surface facing downwards, there is a similarity in behavior. However, in general, the Nusselt number calculated for the cavity is lower than the one obtained for the hot surface facing upwards. This mismatch can be attributed to the effects of the enclosure and the stratification of air inside the cavity. To establish a functional relationship for the Nusselt and Rayleigh numbers, considering the form $Nu = a \cdot Ra^b$ (with a and b being two free parameters), the numerical CFD results for the current problem have been fitted. The fitted correlation, expressed by Eq. (27), is displayed in Fig. 10 (black trace). The fitting process was conducted using non-linear least squares fitting [24] to obtain the best agreement between the correlation and the numerical data.

$$Nu = 7.43 \cdot Ra^{0.094} \tag{27}$$

A detailed description of CFD results is presented for two particular cases in Figs. 11 and 12 This figures illustrate the temperature contour (a) and velocity field (b) for the case where the Rayleigh number is low or high respectively. By comparison, it can be seen that temperature fields are more symmetric in the horizontal direction when temperature is 600 K (Fig. 12). However, in both cases, stratification effects are evident when observing the temperature distribution along the vertical direction. For air velocity contours, it implies that convective cells are non-uniform in space and time, so it is expected that flow will show a higher degree of turbulence. This performance of air inside the cavity justifies the presence of a higher Rayleigh number when the tube temperature is approximately 400 K (Fig. 11). In both cases, the structure of the fluid is similar, but for $T_{tube} = 400\,K$ higher velocity gradient in the convective cells
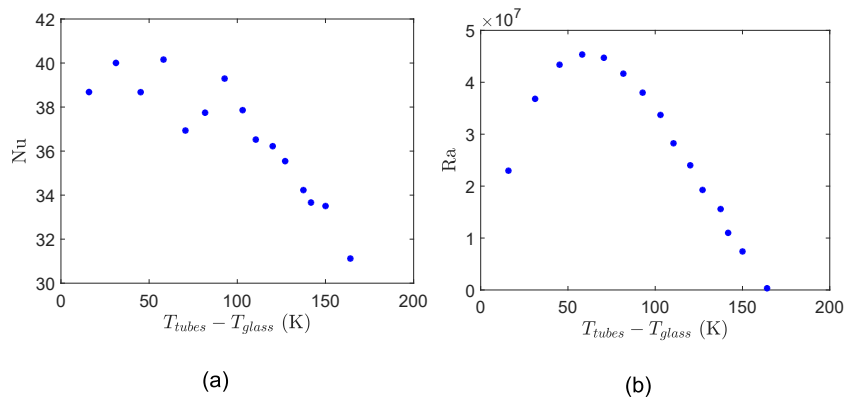
Fig. 8. Nusselt number vs ΔT (a) and Rayleigh number vs ΔT (b).
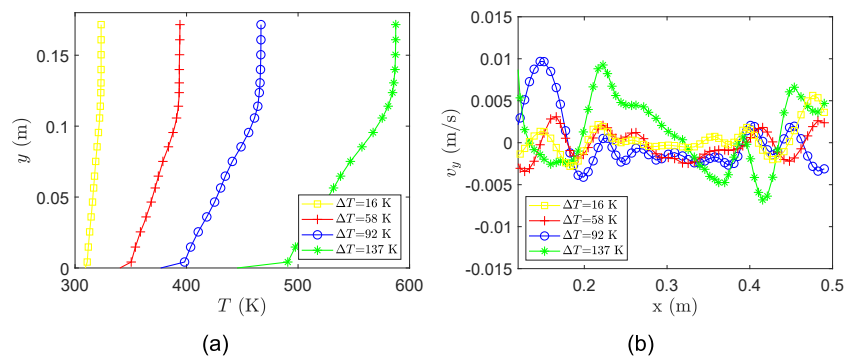

Fig. 9. Temperature profiles across a vertical line (a) and velocity profiles along a horizontal line (b) for selected values of $\Delta T = T_{tubes} - T_{glass}$.
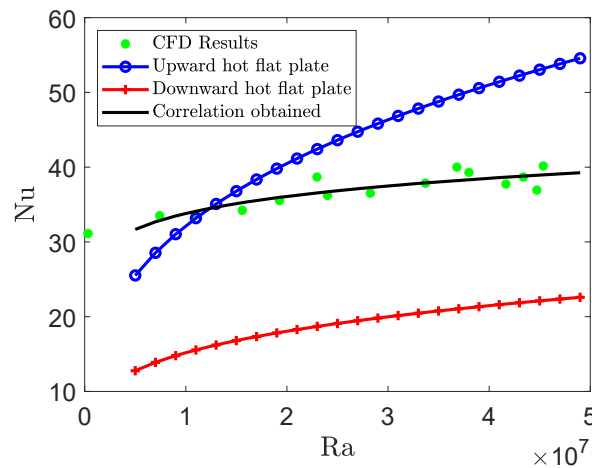

Fig. 10. Nusselt number as a function of the Rayleigh number.

have been reported. For example, in the circulation of the air around the external tubes, where the difference in the magnitude of the velocity vector is more significant compared to the case of $T_{tube} = 600\,K$.

4. Conclusions

In this work, a numerical thermal analysis of a cavity receiver of a linear Fresnel solar collector (LFC) prototype has been proposed. The receiver is formed by arrangement of 6 parallel tubes. On one hand, from the results of a two-dimensional thermal model

(a)

(b)
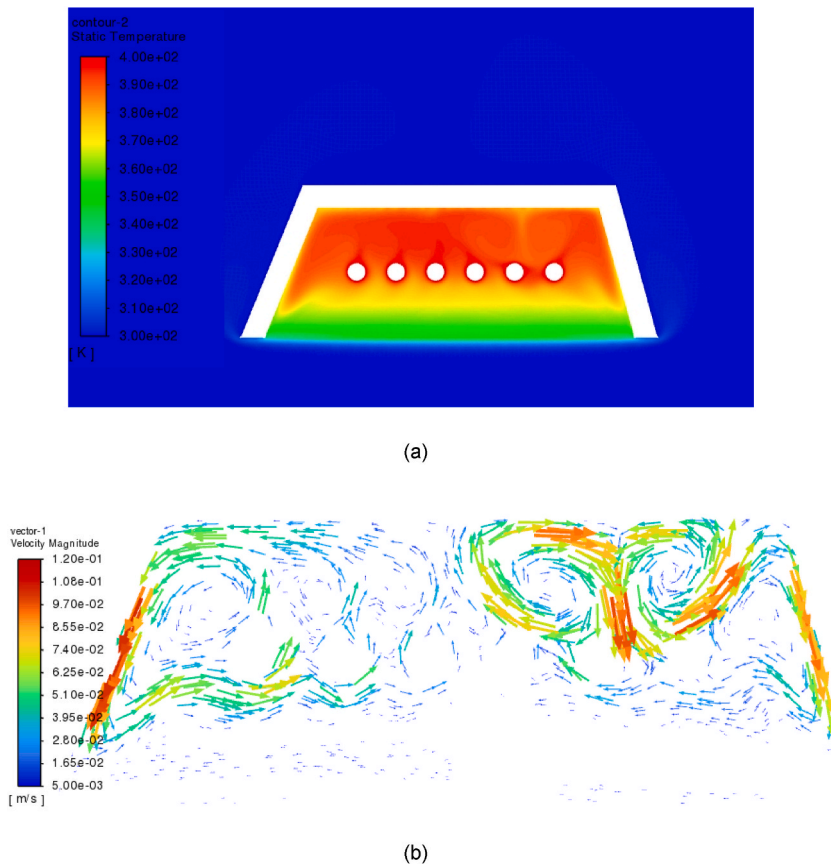
Fig. 11. Contours of air temperature (a) and velocity (b) for $\Delta T = 58$ K ($T_{tubes} = 400\,K$).

implemented in a CFD tool, a set of algebraic correlations has been proposed to accurately approximate heat losses in the receiver from the surface temperature of the tubes. On the other hand, a non-dimensional analysis has been carried out to gain a better understanding of the thermal performance and how the flow behaves inside the cavity. Velocity field and temperature contour have also been presented.

First, it is worth mentioning that a sufficiently large mesh is advisable to reproduce the natural convection phenomenon. It has been implemented this way to guarantee that the far field boundary conditions do not significantly affect the convective transport around the cavity. Fig. 2 shows the dimensions of the mesh adopted. With regard to the heat transfer mechanism in the receiver cavity, it has been found that radiative losses account for 81% of the total heat losses. Considering the operating conditions of the system, this was expected because the glass window closing the cavity aperture, significantly limits convective losses. From the constructive and operational point of view, as shown in section 3.1.1, outer tubes temperature has been found to be the main responsible for heat losses. To reduce them, T_3 must be as lower as possible. For this reason, in real applications with this design of the LFC receiver cavity and tubes bundle, it is recommended that the heat transfer fluid enters the receiver through the two outer tubes of the bundle and exits the receiver through the two central tubes.

Finally, to complete a comparative analysis of the convective transport inside the cavity, a non-dimensional analysis has been carried out. As shown in Fig. 10, it behaves similarly to an analogous problem in which the air moves with a hot plate located on the upper part, and the temperature of the cold source is the average temperature of the air in the lower part of the cavity. Knowing this, a correlation has been obtained to relate the Nusselt and Rayleigh numbers, which allows us to predict convective heat transfer inside the cavity from the surface temperature of the absorber tubes.

This work is useful to predict heat losses in an installation with a low longitudinal gradient of temperature from tube temperature (as it has been made for validation, where the temperature of tubes is constant and known), and also, will be useful to be applied as a boundary condition in a simulation of an installation composed by this receiver. Nevertheless, it has been assumed that the cross-sectional temperature distribution of tubes is constant, so, the application of this model always implies an error that must be quantified. The higher the temperature difference is across the cross section, the higher the error will be. In this sense, in future works, it can be considered to divide tubes into several parts taking into account all the possible combinations of temperatures. It would reduce errors but it would increase computational cost. Besides, it will be of interest to take into account different ambient temperature and air velocities in the surrounding of the receiver for a better knowledge of the impact of these magnitudes on the heat losses.
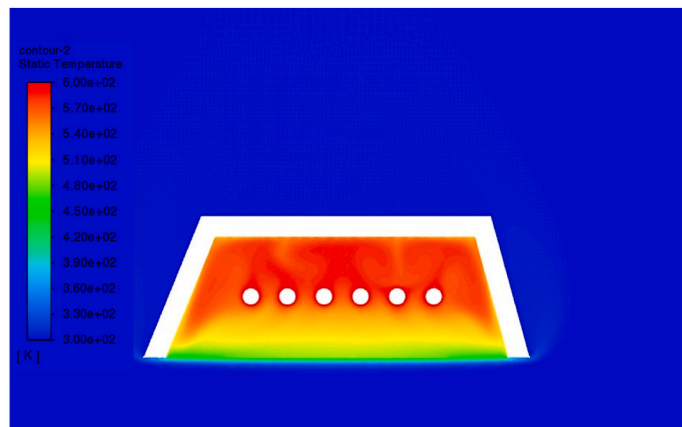
(a)
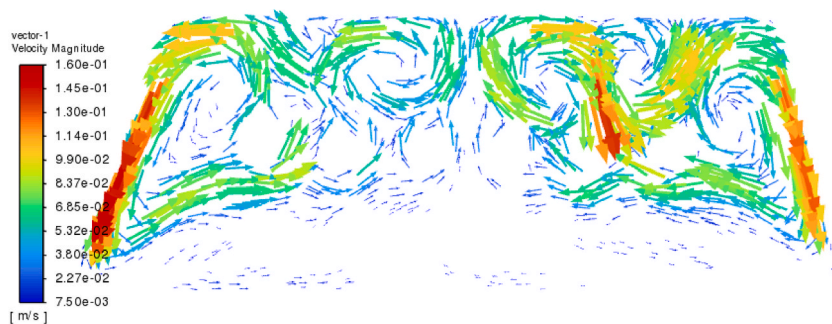
(b)

Fig. 12. Contours of air temperature (a) and velocity (b) for $\Delta T = 137$ K ($T_{tubes} = 600\ K$).

Author contribution statement

Sergio Alcalde-Morales: Conceived and designed the experiments; Performed the experiments; Analyzed and interpreted the data; Wrote the paper.

Loreto Valenzuela: J.J. Serrano-Aguilera: Conceived and designed the experiments; Analyzed and interpreted the data; Contributed reagents, materials, analysis tools or data; Wrote the paper.

Data availability statement

Data will be made available on request.

Declaration of competing interest

The authors declare that they have no known competing financial interests or personal relationships that could have appeared to influence the work reported in this paper

Acknowledgments

Nomenclature

Symbols

a	free parameter for Nusselt correlation
b	free parameter for Nusselt correlation
C_f	friction coefficient
C_i	coefficient i
e	internal energy (J/(mol·K))
g	gravity (m/s^2)
h	air enthalpy (J/(mol·K))
k	thermal conductivity (J/(mol·K))
L_c	characteristic length (m)
M	molar mass of air (g/mol)
Nu	Nusselt number
q	heat flux through a surface (W/m)
R	constant of ideal gas (J/(mol·K))
Ra	Rayleigh number
S	Sutherland's temperature (K)
T	temperature (K)
t_i	tube i
T_i	temperature of tube i (K)
T_{pipe}	mean temperature of the tubes (K)
U_∞	characteristic velocity (m/s)
U_τ	characteristic transverse velocity (m/s)
v	air velocity (m/s)
y^+	mesh characterization parameter

Greek letters

α	thermal diffusivity (m^2/s)
ε	emissivity ($-$)
ρ	density (kg/m^3)
υ	kinematic viscosity (m^2/s)
μ	dynamic viscosity (kg/(m·s))
τ	stress tensor (N)

Subscript

amb	ambient
c	convection
$cavity$	air in the receiver cavity
$glass$	glass cover
i	natural number
$inner$	inner side wall of the receiver cavity
r	radiation

Acronyms

CFD	computational fluid dynamics
LFC	linear Fresnel collector
MAE	mean absolute error
OD	outer diameter
PSA	Plataforma Solar de Almería
RNG	Re-Normalization group theory

References

[1] G. Zhu, T. Wendelin, M.J. Wagner, C. Kutscher, History, current state, and future of linear Fresnel concentrating solar collectors, Sol. Energy 103 (2014) 639–652.

[2] W.J. Platzer, D. Mills, W. Gardner, Linear Fresnel Collector (LFC) solar thermal technology, in: Concentrating Solar Power Technology, Elsevier, 2021, pp. 165–217.

[3] D.J. Reynolds, M.J. Jance, M. Behnia, G.L. Morrison, An experimental and computational study of the heat loss characteristics of a trapezoidal cavity absorber, Sol. Energy 76 (2004) 229–234.

[4] P.L. Singh, R.M. Sarviya, J.L. Bhagoria, Heat loss study of trapezoidal cavity absorbers for linear solar concentrating collector, Energy Convers. Manag. 51 (2010) 329–337.

[5] A. Saxena, N. Jhamaria, S. Singh, S.S. Sahoo, Numerical analysis of convective and radiative heat losses from trapezoidal cavity receiver in LFR systems, Sol. Energy 137 (2016) 308–316.

[6] J. Facão, A.C. Oliveira, Simulation of a linear Fresnel solar collector concentrator, Int. J. Low Carbon Technol. 5 (2010) 125–129.

[7] R. Manikumar, A. Valan Arasu, Heat loss characteristics study of a trapezoidal cavity absorber with and without plate for a linear Fresnel reflector solar concentrator system, Renew. Energy 63 (2014) 98–108.

[8] S.K. Natarajan, K. Reddy, T.K. Mallick, Heat loss characteristics of trapezoidal cavity receiver for solar linear concentrating system, Appl. Energy 93 (2012) 523–531.

[9] K.S. Reddy, K.R. Kumar, Estimation of convective and radiative heat losses from an inverted trapezoidal cavity receiver of solar linear Fresnel reflector system, Int. J. Therm. Sci. 80 (2014) 48–57.

[10] O.A. López-Núñez, J.A. Alfaro-Ayala, O.A. Jaramillo, J.J. Ramírez-Minguela, J.C. Castro, C.E. Damian-Ascencio, S. Cano-Andrade, A numerical analysis of the energy and entropy generation rate in a Linear Fresnel Reflector using computational fluid dynamics, Renew. Energy 146 (2020) 1083–1100.

[11] N. Velázquez, O. García-Valladares, D. Sauceda, R. Beltrán, Numerical simulation of a linear Fresnel reflector concentrator used as direct generator in a solar-GAX cycle, Energy Convers. Manag. 51 (2010) 434–445.

[12] D. Pulido-Iparraguirre, L. Valenzuela, J.-J. Serrano-Aguilera, Fernández-García, Optimized design of a linear Fresnel reflector for solar process heat applications, Renew. Energy 131 (2019) 1089–1106.

[13] D. Pulido, Desarrollo de un prototipo de captador solar Fresnel lineal de media temperatura, Ph.D Thesis, University of Almería, Spain, 2020.

[14] J. Fernández-Reche, L. Valenzuela, D. Pulido-Iparraguirre, Measuring concentrated solar radiation flux in a linear Fresnel-type solar collector, Solar 2 (2022) 401–413.

[15] ANSYS Fluent, Fluid Simulation Software, 2021. http://www.ansys.com/products/fluids/ansys-fluent.

[16] S.A. Suslov, S. Paolucci, Nonlinear analysis of convection flow in a tall vertical enclosure under non-Boussinesq conditions, J. Fluid Mech. 344 (1997) 1–41.

[17] T.M. Squires, S.R. Quake, Microfluidics: fluid physics at the nanoliter scale, Rev. Mod. Phys. 77 (2005) 977. https://doi.org/10.1103/RevModPhys.77.977.

[18] Sixin Fan, Budugur Lakshminarayana, Mark Barnett, Low-Reynolds-number k-epsilon model for unsteady turbulent boundary-layer flows, AIAA J. 31 (10) (1993) 1777–1784.

[19] Vittorio Michelassi, Wolfgang Rodi, J. Zhu, Testing a low-Reynolds number k-epsilon turbulence model based on direct simulation data, AIAA J. 31 (9) (1993) 1720–1723.

[20] J.P.V. Doormaal, G.D. Raithby, Enhancements of the simple method for predicting incompressible fluid flows, Numer. Heat Tran. 7 (1984) 147–163.

[21] S.F. Larsen, M. Altamirano, A. Hernández, Heat loss of a trapezoidal cavity absorber for a linear Fresnel reflecting solar concentrator, Renew. Energy 39 (2012) 198–206.

[22] Y.A. Çengel, A.J. Ghajar, Transferencia de calor y masa: fundamentos y aplicaciones, fourth ed., McGraw-Hill Interamericana, 2011.

[23] T.L. Bergman, A.S. Lavine, F.P. Incropera, D.P. DeWitt, Introduction to Heat Transfer, John Wiley & Sons, 2011.

[24] M.P. Ng, G.K. Grunwald, Nonlinear regression analysis of the joint regression model, Biometrics (1997) 1366–1372.